Chaos, Solitons & Fractals 50 (2013) 48–64

Contents lists available at SciVerse ScienceDirect

Chaos, Solitons & Fractals

Nonlinear Science, and Nonequilibrium and Complex Phenomena

journal homepage: www.elsevier.com/locate/chaos

Multicellular models of intercellular synchronization in circadian neural networks

Michael A. Henson *

Department of Chemical Engineering, University of Massachusetts, Amherst, MA 01007, United States

ARTICLE INFO

Article history:
Available online 8 January 2013

ABSTRACT

The circadian clock generates 24 h rhythms that drive physiological and behavioral processes in a diverse range of organisms including microbes, plants, insects, and mammals. Recent experimental advances have produced improved understanding of the molecular mechanisms involved in circadian rhythm generation at the single cell level. However, the intercellular mechanisms that allow large populations of coupled pacemaker cells to synchronize and coordinate their rhythms remain poorly understood. The purpose of this article is to review recent progress in dynamic modeling of the circadian clock with a focus on multicellular models required to describe cell population synchronization. Mammalian systems are emphasized to illustrate the highly heterogeneous structure and rich dynamical behavior of multicellular circadian systems. Available multicellular models are characterized with respect to their single cell descriptions, intercellular coupling mechanisms, and network topologies. Examples drawn from our own research are used to demonstrate the advantages associated with integrating detailed single cell models within realistic multicellular networks for prediction of mammalian system dynamics. Mathematical modeling is shown to represent a powerful tool for understanding the intracellular and intercellular mechanisms utilized to robustly synchronize large populations of highly heterogeneous and sparsely coupled single cell oscillators. The article concludes with some possible directions for future research.

1. Introduction

The circadian clock generates 24 h rhythms that provide robust regulation of a variety of physiological and behavioral processes in a diverse range of organisms, such as the fungus *Neurospora* [65,78], the plant *Arabidopsis* [105], the fly *Drosophila* [46,48], and mammals [99,100,133]. Recent advances in the understanding of the molecular basis for circadian rhythms have revealed details on the organization of circadian systems at the single-cell level [110]. However, the intercellular mechanisms that allow large populations of oscillatory neurons to synchronize and coordinate their rhythms are not well understood. Experimental evidence strongly suggests that robustness in timekeeping precision emerges in the collective behavior and not at the single-cell level [50]. The study of coupled biological oscillators has attracted considerable attention [38,132] and is part of a broader movement towards research on complex network systems [113]. Such systems are intrinsically difficult to understand because network nodes are high dimensional, network connectivity is heterogeneous across the population, and wiring between nodes can change over time.

In mammals, the suprachiasmatic nucleus (SCN) of the hypothalamus is the dominant circadian pacemaker that drives daily rhythms in behavior and physiology [59]. Experimental studies demonstrate that SCN neurons can sustain circadian rhythms without periodic input and indicate that a pacemaker within the SCN is required to drive near 24-h rhythmicity in other regions of the brain [1,117]. Individual SCN neurons in *in vitro* cultures can express firing rate rhythms with different periods [51,71].

* Tel.: +1 413 545 3481; fax: +1 413 545 1647.
E-mail address: henson@ecs.umass.edu

0960-0779/$ - see front matter © 2012 Elsevier Ltd. All rights reserved.
http://dx.doi.org/10.1016/j.chaos.2012.11.008

These results show that the SCN is a multioscillator system and suggest that individual SCN cells can act as autonomous circadian pacemakers. *In vivo*, these cells must synchronize to environmental cycles and to each other. Although intercellular communication within the SCN has been the focus of significant experimental effort, little is known about how SCN cells synchronize to each other to coordinate behavior [9,72].

Mathematical modeling of circadian rhythm generation has been proposed as a means to understand the design principles of circadian systems in particular and coupled biological oscillators more generally. A number of mathematical models for the circadian clocks in *Neurospora* [32,40,68,103,108], *Drosophila* [37,40,66,108,118,119], and mammals [31,67,80], and more recently in cyanobacteria [104] and plants [97], have been presented. These single cell oscillator models range from simple limit cycle oscillators [6] to detailed descriptions of interconnected transcriptional and translational feedback loops [31,80] to Hodgkin–Huxley type models of neuron electrophysiology [107]. Modeling of circadian neuron populations for the purpose of studying synchronization also has received substantial attention. Conceptual models constructed from simple differential equation models of an oscillating neuron and phenomenological descriptions of intercellular coupling have been proposed for studying circadian rhythm generation [4,6,39,62,71,90]. While conceptually appealing and computationally efficient, such models cannot be directly related to specific molecular events. Multicellular models based on more mechanistic descriptions of circadian gene regulation have been presented for *Drosophila* [27,96,120], the cockroach *Leucophaea maderae* [96], and more recently for mammals [15,41,116].

The purpose of this article is to review recent progress in multicellular modeling of the circadian clock with a focus on mammalian systems due to their clear relevance to human health and performance. First a brief overview of experimental studies on the mammalian circadian clock is provided to demonstrate the heterogeneous structure and rich dynamical behavior of this multicellular system. Then a summary of available multicellular models is presented to distinguish the broad range of modeling approaches and to illustrate the associated modeling challenges and opportunities. Examples drawn from our own research are used to demonstrate the advantages associated with integrating detailed single cell models within realistic multicellular networks for prediction of mammalian circadian behavior. Finally, some possible directions for future research are outlined.

2. The mammalian circadian clock

Due its impact on various mood [75,102] and sleep disorders [60,133] in humans, the mammalian circadian system has been widely studied through both experimental and modeling approaches. The objective of this section is to summarize the current state of knowledge about the mammalian circadian system with regards to its heterogeneous structural features and complex dynamical behaviors as a prelude to the modeling studies described in the subsequent sections. In mammals, most physiological and behavioral events are subject to well controlled daily oscillations generated by an internal self-sustained master clock located in the suprachiasmatic nucleus (SCN) of the hypothalamus. The SCN clock consists of approximately 20,000 individual neurons whose activities are coordinated to produce 24 h cycles in gene expression and firing frequency [130]. The complexity of the SCN network arises not only from its large size but also from the complex dynamic behavior of each neuron and the heterogeneous topology connecting individual neurons.

2.1. Single cell oscillations

Oscillations at the single cell level are produced by a well characterized gene regulatory network that involves a number of interlocking positive and negative feedback loops in which three *Period* (*Per*) and two Cryptochrome (*Cry*) genes genes occupy central positions [100]. As part of the core transcription-translation negative feedback loop, PER and CRY proteins synthesized in the cytosol form PER–CRY dimers that are transported into the nucleus. Two transcription factors CLOCK and BMAL1 synthesized in the cytosol are transported into the nucleus to form CLOCK–BMAL1 dimers that activate transcription of the *Per* and *Cry* genes and inhibit transcription of the *Bmal1* gene. This activation is rhythmically suppressed and reestablished by PER–CRY dimers, which block the activity of CLOCK–BMAL1 dimers and negatively autoregulate transcription of the *Per* and *Cry* genes. With the exception of CLOCK and the CLOCK–BMAL1 dimer, each protein and protein complex can be phosphorylated and subsequently degraded. Activation is rhythmically suppressed and restored approximately every 24 h as the inhibitory PER and CRY proteins accumulate and then degrade.

Circadian modulation of neural firing causes a number of electrophysiological properties of the cell membrane to fluctuate over the course of the day [19]. *In vitro* studies of the SCN have demonstrated daily modulation of neural firing [53], resting potential [61] and membrane resistance [95], as well as daily oscillations in a number of ionic currents [55,77]. A direct association between membrane excitability and core-clock rhythms has been reported, providing evidence for a positive correlation between *Per* gene transcription and firing frequency [89,98].

2.2. Cellular and network heterogeneity

The SCN consists of a broad range of neural subgroups, typically differentiated according to their neuropeptide content [122], their afferent [81] and efferent [64] connections with other regions of the brain, and their oscillatory behavior [64,106]. Morphological studies in a variety of mammals [3,22] have demonstrated that the SCN is organized into two structurally and functionally distinct subdivisions. The two regions, differentiated based on their neuropeptide content and network architecture, have been designated as the “core” and the “shell” [3,101]. The core refers to the ventral region of the nucleus comprised of approximately 40% of all SCN neurons. Core neurons

primarily produce vasoactive intestinal peptide (VIP) co-localized with γ-aminobutyric acid (GABA) [82,83]. The shell surrounds the core and contains approximately 60% of the SCN cell population. Shell neurons primarily produce arginine vasopressin (AVP) [56] co-localized with GABA [82,83]. Synaptic connections within the shell are confined mostly between proximal neurons [94,111]. By contrast, axons originating from VIP synthesizing cells of the core extend densely over the entire SCN establishing synaptic connections between core neurons [26] as well as with shell neurons [56]. Further contributing to heterogeneity of the circadian network, SCN neurons differ in their intrinsic rhythmic behavior in the absence of cell-to-cell communication. Treatments that desynchronize rhythms among SCN neurons have revealed that only 30% of the population behaves as self-sustained oscillators [10].

2.3. Intercellular signaling

Circadian rhythmicity is ensured not only by autonomous intracellular mechanisms within individual cells [100] but also by intercellular communication that coordinates functionally and structurally distinct cell types across the SCN [42,72]. Studies have shown that VIP is a critical neuropeptide involved in the generation and synchronization of circadian rhythms [9]. VIP is synthesized in the core by approximately 10–20% of the 20,000 SCN neurons, while the VIP receptor VPAC2 is expressed by 60% of the neurons across the SCN [58]. Mice lacking VIP [54] or VPAC2 [47] have been reported to express multiple circadian rhythms or single rhythms with greatly reduced periods and lower amplitude oscillations than wild-type mice [9,17,18]. While the 70% of wild-type SCN neurons that fired in a circadian pattern displayed similar periods and phases, only 30% of VIP and VPAC2 deficient neurons produced daily oscillations and these oscillatory neurons displayed a significantly broader range of periods [9]. The ubiquitous neurotransmitter GABA interacts with $GABA_A$ and $GABA_B$ receptors, producing inhibitory responses through membrane hyperpolarization that effectively shunts transmembrane voltage shifts [23,82,83]. In the case of $GABA_A$ receptors, GABA binding produces hyperpolarization by increasing chloride flow into the neuron [14,24]. A continuing point of controversy concerns the role of GABA in synchronization of the SCN network. Although daily application of exogenous GABA has been shown to synchronize firing rhythms of dispersed SCN neurons [70], GABA blockade had no effect on synchronization and was not required for the expression of a coherent signal within SCN slices [11].

The mechanism by which single cells produce synchronized rhythms in neural firing, gene expression, and neuropeptide secretion is believed to involve intracellular signaling instigated by cytosolic calcium [115]. Calcium is a second messenger that affects not only core-clock transcriptional mechanisms, but also electrophysiological properties of the circadian system. Cytosolic calcium has been demonstrated to activate Ca^{2+}/calmodulin dependent kinases, which in turn phosphorylate the cAMP-response-element binding (CREB) protein, ultimately leading to *Per1* gene induction [115]. Decreased Ca^{2+}concentrations have been shown to abolish daily *Per1* mRNA oscillations in SCN slices [73].

2.4. Light stimulation

One of the most important attributes of the SCN is its ability to perceive photic signals and adapt its periodicity to various light and dark schedules. The core receives direct photic input, as retinohypothalamic tract (RHT) projections have been shown to terminate almost exclusively within the ventral region of the SCN overlapping the distribution of VIP synthesizing neurons [82–84]. By contrast, the shell does not receive direct photic input but rather is entrained by light through long-range synaptic connections from core neurons. Light sensing is primarily achieved via glutamate and pituitary adenylate cyclase activating peptide (PACAP) neurotransmitters released within the retinorecipient core region [44]. Stimulation of glutamate receptors is associated with increased calcium influx [35], which has been shown to activate a number of protein kinases that ultimately induce core-clock gene transcription [93] via activation of CREB [36]. Upon bindings its receptors, PACAP has been shown to instigate a signaling cascade involving a cAMP/protein kinase dependent pathway [43], which in turn stimulates the phosphorylation of CREB and ultimately induces core-clock gene expression [127].

3. Multicellular models of circadian rhythm generation

The circadian core clock is inherently complex due to its highly heterogeneous properties, which include neuropeptide content, uncoupled rhythmicity, and photic input at the single cell level and connectivity type, directionality, and strength at the cell population level. Mathematical modeling of the core clock offers the potential to integrate existing knowledge and to generate experimentally testable hypotheses about system dynamics and function. While single neuron models can provide insights into the molecular machinery responsible for individual cell oscillations, they cannot address critical questions about the effects of cellular heterogeneity and intercellular communication on cell population dynamics and collective rhythm generation.

A typical multicellular model of the core circadian clock consists of an ensemble of coupled single cell oscillators. These models can be used to better understand population synchronization and other complex system dynamics that result from intracellular gene regulation, intercellular signaling, and cellular heterogeneity. There is a vast literature on the synchronization of heterogeneous populations of coupled oscillators that has application to circadian rhythm generation [63,79,112,131,132]. A prototypical problem involves a population of limit-cycle oscillators with natural frequencies drawn from a random distribution that are coupled through weighted sinusoidal functions depending on differences between the oscillator phases. In the absence of coupling, each oscillator produces its natural frequency and a coherent overall rhythm is not

observed. When the coupling weight is sufficiently large, the system exhibits a phase transition where some oscillators self-synchronize with complete synchronization observed in the limit of a large coupling weight [112]. While such conceptual models are useful for gaining insights into general synchronization phenomena, they are not sufficiently realistic for understanding circadian system behavior.

Table 1 contains a listing of representative multicellular circadian models that are differentiated with respect to the type and number of single cell oscillators, the intercellular coupling agent and mechanism, and the main focus of the modeling study. Most models have been developed for the mammalian circadian clock, although several studies have been focused on *Drosophila* due to the abundance of experimental data available for this organism. A stochastic model for the reconstructed *in vitro* circadian oscillator in cyanobacteria has recently been proposed [85]. These multicellular models have been most often used to investigate phase synchronization and light entrainment of cell

Table 1
Representative list of multicellular models of the circadian core clock.

Lead author (year)	Cell model	Cell number	Coupling agent	Coupling scheme	Focus
Petri (2001)[a]	Gene regulatory network	2	Doubly phosphorylated PER protein	Bidirectional	Period of synchronization populations
Oda (2002)[a]	Limit cycle oscillator	2	Coupling weights	Bidirectional	Spitting of oscillator populations in constant light
Ueda (2002)[a]	Gene regulatory network	100	Various	Local	Effect of coupling mechanisms on synchronization
Antle (2003)	van der Pol oscillator	1000	Gating mechanism	Phase resetting	Synchronization of heterogeneous populations
Kunz (2003)	Van der Pol oscillator	100–10,000	Coupling weights	Local	Synchronization of heterogeneous populations
Gonze (2005)	Goodwin oscillator	10,000	Generic neurotransmitter	Mean field	Synchronization & light entrainment
Bush (2006)	Leaky integrate & fire	20–100	Generic neurotransmitter	Local, global, small-world networks	Synchronization of conceptual single cell model
Antle (2007)	van der Pol oscillator	200	Gating mechanism	Phase resetting	Light entrainment of heterogeneous populations
Bernard (2007)	Gene regulatory network	6–309	Generic neurotransmitter	Random, local, & their combination	Effect of network topology & cell number on synchronization
To (2007)	Gene regulatory network	400	VIP signaling network	Local	Synchronization of heterogeneous populations
Diekman (2009)	Integrate & fire	10,000	GABA with coupling weight	Variable connectivity from 0% to 100%	Effect of connectivity on synchronization
Gu (2009)	Goodwin oscillator	1001	Generic neurotransmitter with distributed coupling strength	Mean field	Effect of coupling strength on period distribution
Li (2009)	Goodwin oscillator	30	Generic neurotransmitter	Unconnected & global	Synchronization & light entrainment of core & shell regions
Ullner (2009)	Goodwin oscillator	10,000	Generic neurotransmitter	Mean field	Synchronization with variable coupling strengths
Vasalou (2009)	Gene regulatory network	400	VIP signaling network	Small-world	Synchronization & light entrainment of small-world networks
Abraham (2010)	Poincare oscillator	2	Coupling weight	Mean field	Effect of intracellular coupling on light entrainment
Nagai (2010)[b]	Protein interaction network	2	KaiC protein	KaiC monomer shuffling	Synchronization of mixed samples with different phases
Fukuda (2011) [33]	Phase oscillator	800–8000	Coupling weight	Mean field	Phase wave generation & synchronization
Komin 2011	Goodwin oscillator	200–1000	Generic neurotransmitter	Mean field	Effect of cellular heterogeneity on synchronization & light entrainment
Oda (2011)[a]	Limit cycle oscillator	2	Coupling weights	Bidirectional	Entrainment by two independent *zeitgebers*
Vasalou (2011)	Gene regulatory network	400	VIP & GABA signaling networks	Small-world	VIP & GABA mediated synchronization
Vasalou (2011)	Gene regulatory network	425	VIP & GABA signaling networks	Combination of small-world & local	Synchronization of core & shell regions
Diambra (2012)[a]	Gene regulatory network	50	Doubly phosphorylated PER protein	Mean field	Effect of PER nuclear transport & non-photic PER degradation
Hafner (2012) [41]	Gene regulatory network	200	Generic neurotransmitter	Random, local, & scale-free networks	Effect of network topology on synchronization & light entrainment

All mammalian models unless other indicated.
[a] *Drosophila* models.
[b] Cyanobacteria model.

populations that are heterogeneous with respect to their uncoupled oscillation periods.

The single cell models used in these studies include van der Pol oscillators that simply display oscillatory dynamics, Goodwin oscillators that capture minimal features of the main gene regulatory feedback loop, and more detailed gene regulatory models that capture the interplay between gene products and transcriptional regulation in interlocking positive and negative feedback loops. More detailed single cell models allow the molecular basis of individual cell oscillations and their synchronization to be investigated (e.g. [126]). In principle, synchronization and entrainment of circadian oscillators can be examined with as few as two cells with reciprocal connections (e.g. [96]). Some studies use two oscillators to represent two distinct cellular populations, such as "morning" and "evening" oscillators for capturing splitting of locomotor activity in hamsters [90,91]. Small cell populations can be sufficient to investigate synchronization and entrainment of identical oscillators (e.g. [2]). However, much larger cell populations representative of actual core clocks are required to adequately capture cellular heterogeneity and to compute important population statistics such as the period distribution (e.g. [116]).

With the exception of models that use non-rhythmic "gate" cells to periodically reset the phase of uncoupled oscillator cells (e.g. [6]), the individual oscillators must be coupled to phase synchronize and generate a coherent overall rhythm. A wide variety of intracellular coupling agents and schemes have been proposed to model cell-to-cell communication. A simple approach is to use a single state variable of the oscillator as the coupling agent and to introduce weighted values of this variable from each cell as rhythmic inputs to the other cells. An extension of this coupling weight approach is to assume that each cell synthesizes a generic neurotransmitter (e.g. mimicking VIP in the mammalian clock) and utilizing this neurotransmitter as the coupling agent. More detailed signal transduction models involving the intracellular production and intercellular action of neurotransmitters such as VIP and GABA have been developed for the mammalian circadian clock [116,126].

Several alternative coupling schemes have been proposed for the action of the coupling agent from one cell on the remaining cells in the population. Mean field coupling is based on the assumption that the cellular network is globally coupled (i.e. each cell is connected to every other cell) and that the times scale of coupling agent transmission is fast compared to the 24 h circadian cycle. In this case, the average value of the coupling agent across the cell population multiplied by a coupling weight is used as the input to all cells [33]. In random coupling, each cell is placed on a grid (or possibly a lattice) and connections between cells are assigned randomly according to a chosen probability with all connections having the same coupling weight (e.g. [121]). In local coupling, a particular cell only receives input from cells in close proximity (i.e. nearest neighbors). The coupling weights can have uniform values (e.g. [15]) or vary inversely with the distance between cells (e.g. [62]). Small-world [128] and scale-free [12] network topologies have been proposed as plausible models of the heterogeneous connection patterns observed between circadian neurons. These networks are characterized by a large number of local connections between nearest neighbors and a relatively small number of long-range connections between randomly chosen cells (e.g. [41]) [125]. Combinations of different coupling schemes have been used to model cell-to-cell connectivity observed in the core and shell regions of the mammalian SCN (e.g. [15,124]).

4. Biophysically-based multicellular models of the mammalian circadian clock

While minimal multicellular models of the circadian clock are useful for qualitative analysis, detailed biophysical models offer the possibility of directly connecting molecular interactions to system behavior such as population synchronization and light entrainment. An ideal biophysical model has the following characteristics: (1) a detailed description of the gene regulatory network responsible for single cell oscillations and the electrophysiological mechanisms that allow transmission of cellular information; (2) a plausible description of the signaling network responsible for neurotransmitter release and post-synaptic action; (3) single cell heterogeneity with respect to oscillatory behavior (self-sustained and damped), oscillation period, neurotransmitter release (producing and non-producing), and post-synaptic action (binding and non-binding); and (4) a heterogeneous network topology that captures non-uniform cell-to-cell communication and photic input. This section focuses on multicellular models of the mammalian circadian clock that possess several of these characteristics.

4.1. VIP signaling model of cell-to-cell communication

Experimental studies have demonstrated that the neuropeptide VIP is critical for the generation and synchronization of circadian rhythms [11]. VIP rhythmically released by a particular cell influences another cell by binding its VPAC2 receptors and triggering a signaling cascade that eventually modulates transcription of the *PER* gene in the core clock of the target cell [74]. However, VIP signaling is highly heterogeneous as the neuropeptide is only synthesized by approximately 10–20% of neurons in the core region, while the receptor VPAC2 is expressed by about 60% of neurons across the SCN [58]. When VIP signaling was eliminated in VPAC2 and VIP deficient neurons, only 30% of the neurons produced daily oscillations and they displayed a broad range of periods [11].

Along with Erik Herzog (Washington University) and Frank Doyle (University of California, Santa Barbara), we developed a multicellular model of the mammalian circadian clock that explicitly included VIP signaling [116]. The core oscillator was obtained by modifying a previously published gene regulation model [67] to allow the incorporation of VIP mediated cell-to-cell communication (Fig. 1). While more detailed models of VIP signaling are available [45], we developed a comparatively simple signaling model because the molecular mechanisms involved are not

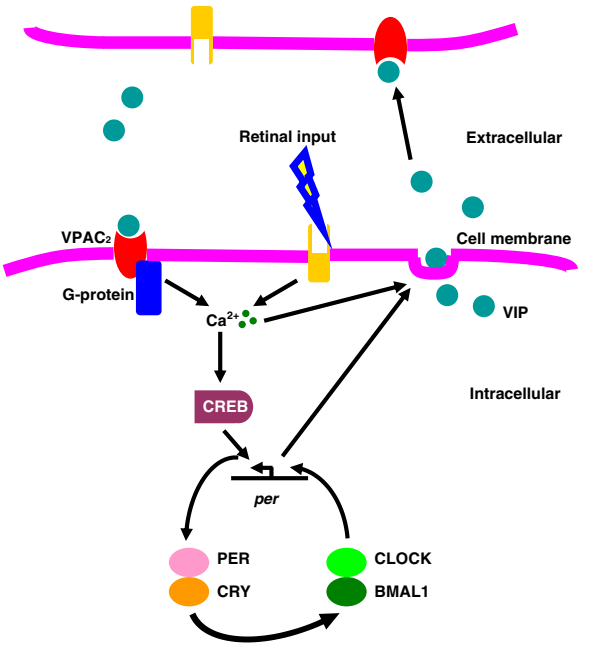

Fig. 1. Schematic representation of VIP mediated cell-to-cell communication used in a multicellular model of the mammalian core clock [116]. A core transcription-translation negative feedback loop provides the drive on rhythmic communication between cells and responds to synchronizing signals from neighboring cells. Within this loop, two transcription factors (CLOCK and BMAL1) form dimers to activate transcription of the *period* gene. This activation is rhythmically suppressed and restored approximately every 24 h as the inhibitory PER and CRY proteins accumulate and then degrade. One hypothesized output of this clockwork is the circadian regulation of VIP release. VIP binds to the G-protein coupled receptor, VPAC2, to increase intracellular calcium and activate CREB. At specific phases in the circadian cycle, activated CREB induces *Per* transcription and shifts the phase of the circadian clock. Increases in intracellular calcium also mediate the phase-resetting effects of light and the release of available VIP.

completely understood. In this signal transduction cascade, VIP was bound by the VPAC2 receptor to increase intracellular calcium and activate the CREB protein, which induced *Per* transcription to modulate the oscillator phase. VIP release in constant darkness was circadian with a constant phase relation to *Per* transcription, while the VIP release rate was assumed to be sufficiently large during constant light to induce complete saturation of VPAC2 receptors. Photic input was further assumed to result in increased intracellular calcium levels. An ensemble of individual cells was placed on a two-dimensional grid, and variable coupling weights that decreased linearly with distance between cells were used to describe non-uniform VIP contributions across the network. End effects on the grid were eliminated by implementing periodic boundary conditions such that neurons located at an edge were connected to corresponding neurons at the opposite side of the grid, thereby producing a symmetric lattice.

Dynamic simulations were performed with 400 cells placed on a 20-by-20 grid, resulting in a multicellular model with 6800 ordinary differential equations. Parameter values for the core oscillator model were obtained from the original Ref. [67], while parameter values associated with VIP signaling were chosen within biologically plausible ranges to mimic experimentally observed synchronization and desynchronization behavior. Asynchronous initial cell states were generated with a previously published method developed for yeast cell population simulations [49]. Each model neuron was assigned a randomly perturbed value of the *Per* mRNA basal transcription rate with 10% standard deviation such that approximately 40% of the neurons produced sustained oscillations in the absence of VIP coupling. To achieve a broad distribution of uncoupled periods, random perturbations with 10% standard deviation were also introduced into eight kinetic parameters associated with the core oscillation model. The instantaneous degree of phase synchrony after each oscillation cycle was quantified with the synchronization index [112], which reflects the synchronization index reflects the instantaneous amplitude of the ensemble rhythm and yields values between zero (no synchronization) and one (perfect synchronization).

The multicellular model was used to investigate the effects of VIP signaling on synchronization dynamics and the distribution of oscillator periods under constant darkness. A highly synchronized initial cell state was generated by simulating the VIP coupled cell ensemble for approximately 10 circadian cycles. To mimic the loss of VIP signaling, the extent of VPAC2 saturation was set to zero at 72 h. Nearly 60% of neurons failed to exhibit rhythmicity two cycles after VIP coupling was eliminated, and synchrony was rapidly lost in the remaining self-sustained oscillators (Fig. 2A). mRNA concentrations were averaged across the cell ensemble to independently assess the effect of VIP signaling on synchrony among cells and the state of their pacemaker mechanism. Rhythms in *Per, Bmal1* and *Cry* mRNAs damped out after approximately three days due to a loss of intracellular rhythmicity and intercellular synchrony (Fig. 2B). While the coupled cell population consisted of 156 self-sustained oscillators with tightly distributed periods and a relatively large average period, loss of VIP signaling reduced the mean period by approximately 5 h and broadened the period distribution (not shown). The synchronization index (SI) exhibited a sharp decrease following VIP removal and eventually settled at a small value indicating a near complete loss of synchrony (Fig. 2C). The model recapitulated experimental findings that removal of VIP signaling leads to a loss of rhythmicity in a majority of cells and reduced synchrony within the SCN of mice, as well as a shortening of the mean circadian period among the remaining rhythmic cells that mimics mice or SCN with disrupted VIP signaling [8,17,18].

The multicellular model was also used to investigate the effect of photic input on circadian synchrony and rhythmicity by exposing the heterogeneous population of 400 cells to different light schedules. The light effect was implemented by increasing the extent of VPAC2 saturation and the light-induced calcium stimulus to their maximum values of unity. Light–dark cycles were simulated by changing these two parameters from their constant light values to their constant dark values every 12 h. Compared to constant darkness, light–dark cycles produced a more coherent overall rhythm with fewer cells that failed to synchronize (Fig. 3A and C). The *Per* mRNA level peaked during

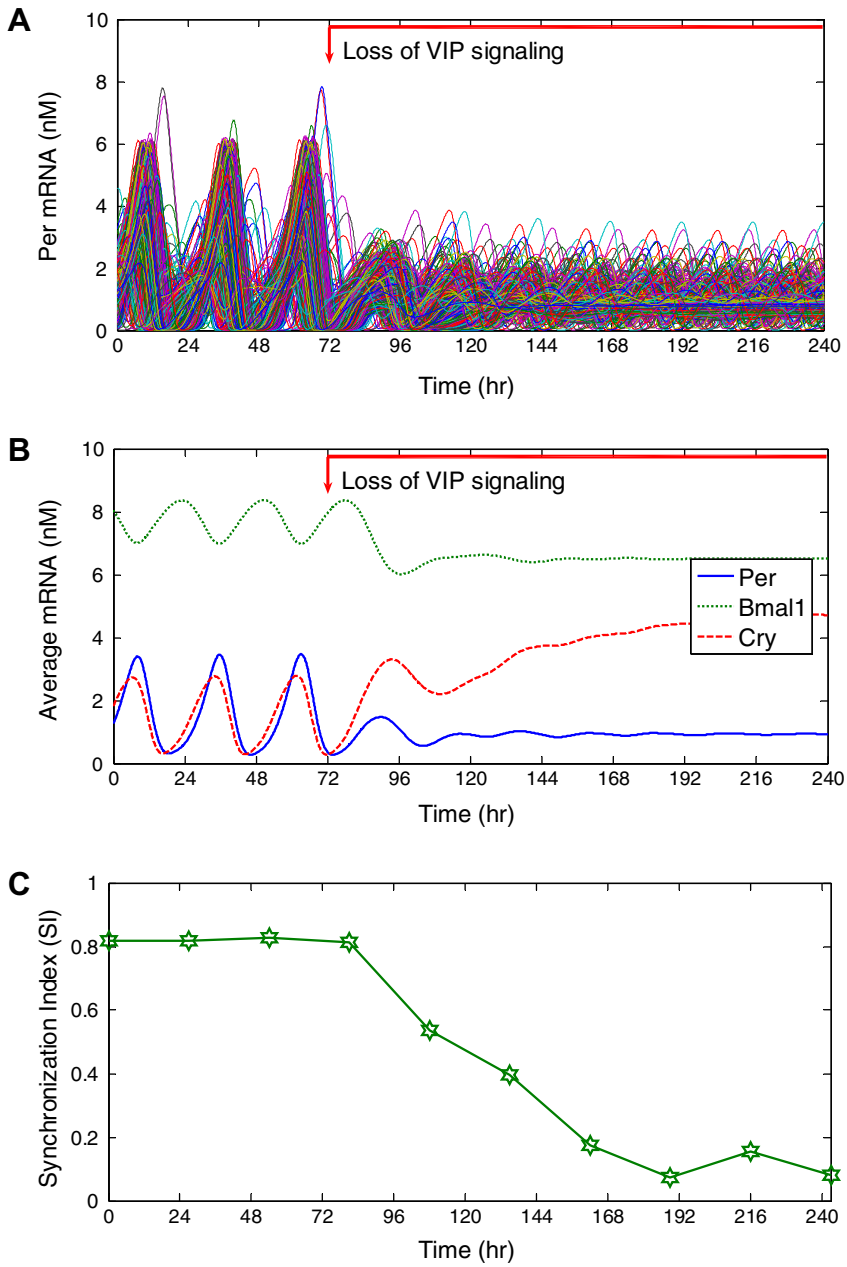

Fig. 2. The effect of eliminating VIP signaling on the synchronization of 400 model neurons under constant darkness [116]. (A) *Per* mRNA dynamics of individual neurons. (B) Ensemble averaged *Per*, *Bmal1*, and *Cry* mRNA dynamics. (C) The synchronization index.

the late day with a period of 24 h, indicating the rhythm had entrained as seen *in vivo* [100]. These results support the experimental observation that entrainment to a 24 h cycle further improves the precision of the ensemble rhythm compared to free running conditions in constant darkness [50]. Although all neurons were rhythmic under constant light, the population failed to synchronize despite intercellular coupling by VIP signaling (Fig. 3B and C). These results may explain data showing that individual SCN cells remain rhythmic in constant light, but lose synchrony with the population [92].

4.2. Small-world network model of intercellular coupling

The complexity of the SCN neural network arises not only from the complex dynamic behavior of each neuron but also from the heterogeneous coupling between individual oscillators. To relate the dynamics of such complex networks to their structural characteristics, techniques have been developed to allow the general mathematical representation of numerous biological and engineered networks [5,113]. Various neural systems in the mammalian brain have been shown to be adequately characterized by

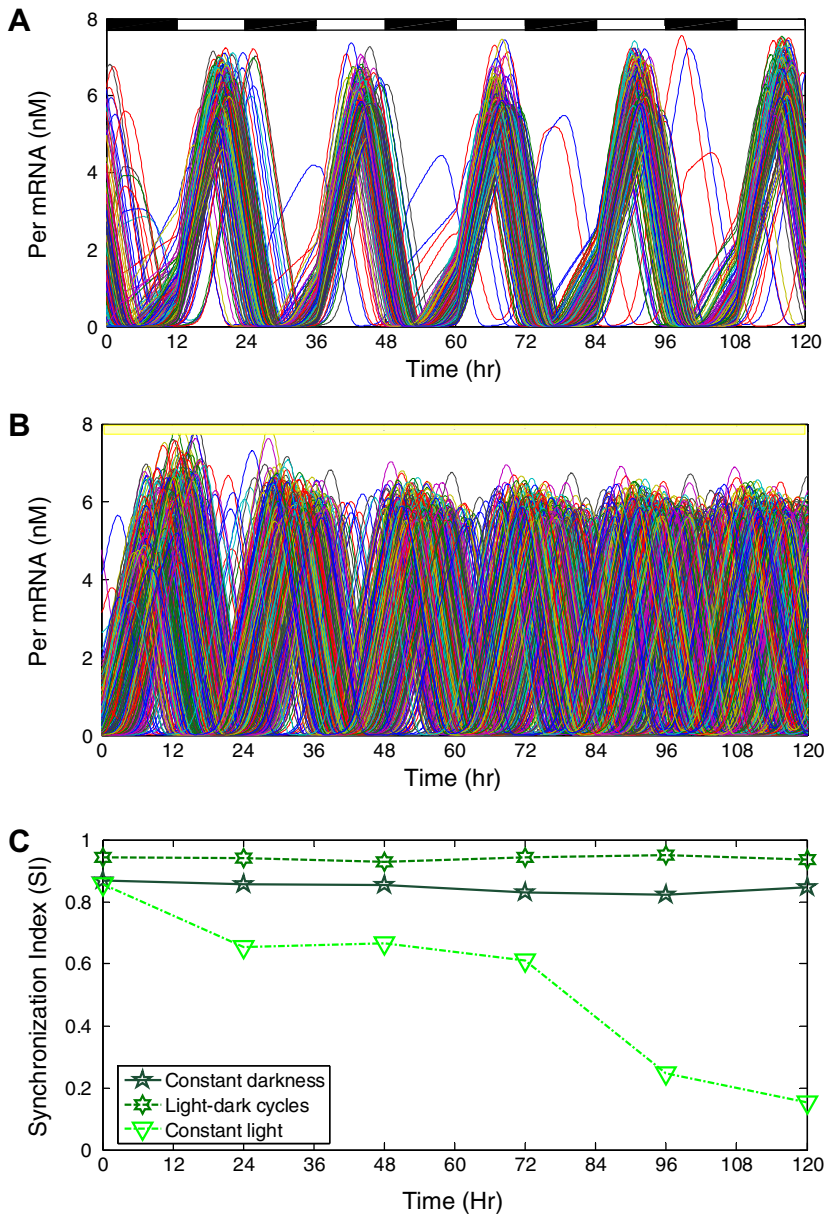

Fig. 3. The effect of photic input on the synchronization of 400 model neurons [116]. (A) Synchronization dynamics under repeated light–dark cycles. (B) Loss of synchronization under constant light. (C) The synchronization index for constant darkness, constant light, and light–dark cycles.

small-world networks [87]. The small-world topology combines local circuits of tightly coupled cells with random connections between cells, thereby introducing long-range connections that substantially reduce the average path length between cells [88,128]. One of the most important attributes of the small-world topology is its ability to produce synchronous signals as readily as globally connected networks for which the mean field assumption is applicable. However, small-world networks contain much lower degrees of interconnectedness than the mean-field model and can considered as low "energy" alternatives.

Small-world [21] and related scale-free [41] network models of the SCN have been developed to investigate synchronization phenomenon. Along with Erik Herzog (Washington University), we developed a multicellular model which incorporated a detailed gene regulatory cell model into a heterogeneous network of coupled oscillators [125]. Our study was motivated by anatomical evidence suggesting the presence of both short-range and long-range VIP mediated connections in the core region of the SCN [26]. Each model cell was described by a detailed gene regulatory network model [67]. Cellular heterogeneities were introduced via random perturbations with 10% standard deviation in the basal *Per* transcription rate such that 40% of the model neurons were self-sustained oscillators and in the *Bmal1* transcription and mRNA degradation

rates with 2% standard deviation such that that distribution of uncoupled periods of the self-sustained oscillators ranged between 18 and 30 h. Intracellular communication was described with the VIP signaling cascade model from our previous study (see Section 4.1) modified such that all synaptic connections had a coupling strength of unity.

Small-world neural networks were constructed through the following procedure, which extended an established method for one-dimensional lattices [88] to the two-dimensional grids. We placed 400 heterogeneous cells on a 20×20 rectangular grid, with each cell connected to its four nearest neighbors to establish local connections (Fig. 4A). Additional connections (referred to as shortcut connections) were established at the beginning of each simulation between random pairs of cells according to a probability p. Extreme values of p produced the nearest neighbor topology ($p = 0$, Fig. 4A) and the fully connected, mean field topology ($p = 1$, Fig. 4C). Intermediate probability values produced networks between these two extremes, with values in the range $0.01 < p < 0.1$ referred to as small-world network topologies [88], Fig. 4B. Following standard graph theory [109], we did not allow multiple connections between the same neuron pairs or connections of a neuron with itself. VIP heterogeneity was captured by randomly zeroing VIP production from 80% of the model neurons and eliminating all connections from these non-VIP producing cells. Therefore, the 20% of VIPergic neurons could establish bidirectional connections, while the 80% of non-VIPergic neurons could only receive connections from other cells (Fig. 4D). For each p value investigated, we constructed 10 network realizations for statistical calculation of structural and dynamic network properties. In addition to the synchronization index (SI), we calculated the order parameter (R) [34] for the overall degree of synchrony over the specific time period of 200 h.

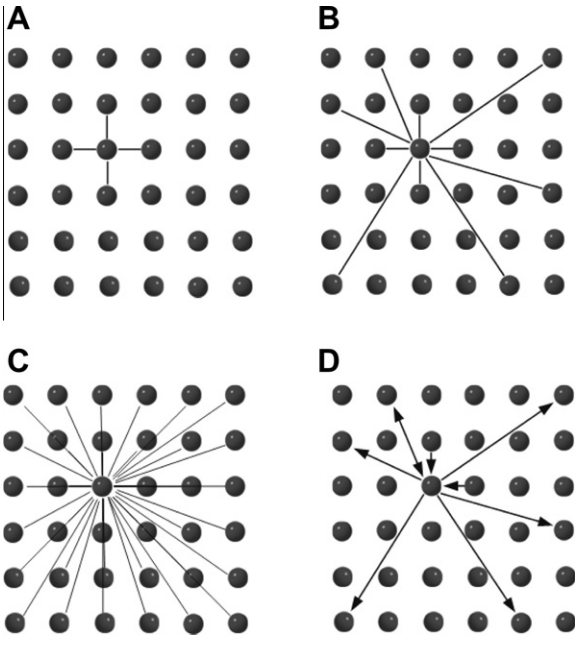

Fig. 4. Schematic representation of SCN network topologies on a two-dimensional grid [125]. (A) Nearest neighbor network with each neuron connected to its four nearest neighbors. (B) Small-world network with additional shortcut connections added to the nearest neighbor network according to a probability p. (C) Mean field network with each neuron connected to every other neuron. (D) The small-world network that results when VIP production is randomly eliminated from a fixed percentage of neurons, yielding a heterogeneous network with both reciprocal and non-reciprocal connections.

We varied the probability p to determine the effect of adding shortcut connections on the synchronization behavior of different network architectures under constant darkness. *Per* mRNA time profiles of 10 randomly selected cells showed that limited long range connectivity across the small-world network ($p = 0.05$) eliminated arrhythmic cells and produced a highly phase synchronized population (Fig. 5A). The predicted SI value of 0.93 obtained at the end of the simulation was close to the SI value of 0.90 calculated from SCN slice data (data not shown). By contrast, the nearest neighbor model ($p = 0$) with no long range connections produced a fraction of arrhythmic cells and a poorly phase synchronized population (Fig. 5B). Rapid and nearly complete synchronization was observed for both the small-world ($p = 0.05$) and mean field ($p = 1$) models (Fig. 5C). While the small-world networks obtained for $p = 0.01$ exhibited a rapid increase in SI following coupling, the extent of long range coupling was not sufficient to achieve the same degree of synchronization as obtained for larger p values. Despite its extensive local coupling, the nearest neighbor model ($p = 0$) was not able to produce a well synchronized population and exhibited greater variability in SI values with time. The probability p had similar effects on SI values computed at the end of eight cycle simulations and R values computed over the last eight cycles of these simulations, suggesting that the effective dynamic range of the small-world network was $0.001 < p < 0.05$ (Fig. 5D). Comparatively small standard derivations in the synchronization measures were obtained for $p > 0.05$, showing that the small-world networks were able to consistently synchronize the cell populations despite cellular and network heterogeneities.

We varied the probability p for different light schedules to determine their combined effects on network synchronization behavior. Three schedules were considered: constant darkness (DD), constant light (LL), and 12 h of constant light followed by 12 h of constant darkness (LD). As in our previous model [116], photic input was assumed to enhance *Per* transcription through the VIP signaling cascade. The DD results repeated from Fig. 5D show that a highly synchronized population was only achieved for p values in and above the small-world region including our nominal value $p = 0.05$ (Fig. 6). LD cycles produced larger SI values regardless of the p value, suggesting that long range connections were less critical under conditions of light entrainment. By contrast, LL failed to produce a synchronized population regardless of the p value. Such behavior is supported by experiments in which exposure to constant bright light abolished circadian synchrony across the population [92]. Our results suggest that the primary advantage of small-world networks is to promote synchronization among sparsely connection populations in the absence of light.

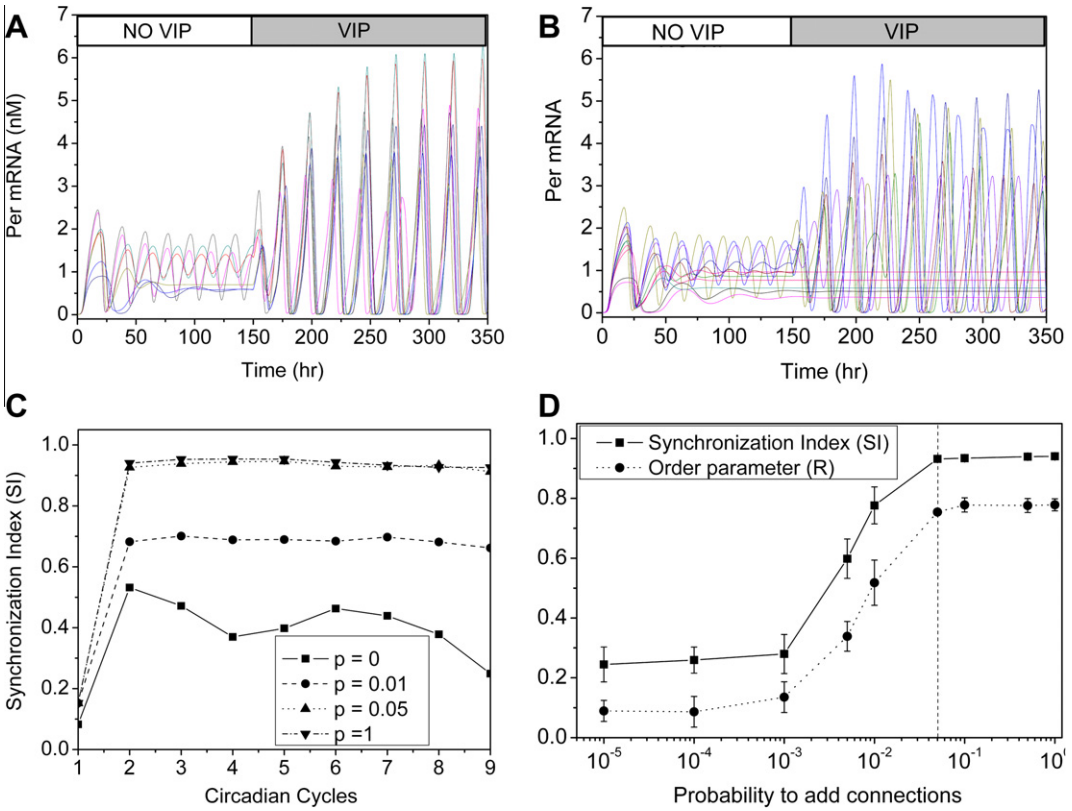

Fig. 5. Synchronization behavior of SCN network topologies when VIP was introduced at 150 h [125]. (A) *Per* mRNA time profiles of 10 randomly selected cells for a small-world network model ($p = 0.05$). (B) *Per* mRNA time profiles of 10 randomly selected cells for the nearest neighbor model ($p = 0$). (C) Synchronization index (SI) versus time for four values of the probability p, where circadian cycle 1 represents the time of VIP introduction. (D) Final SI values computed at the end of eight cycles and R values computed over the last eight cycles as a function of the probability p. For each p value, mean SI and R values (circles) and their standard deviations (error bars) were computed from 10 network realizations.

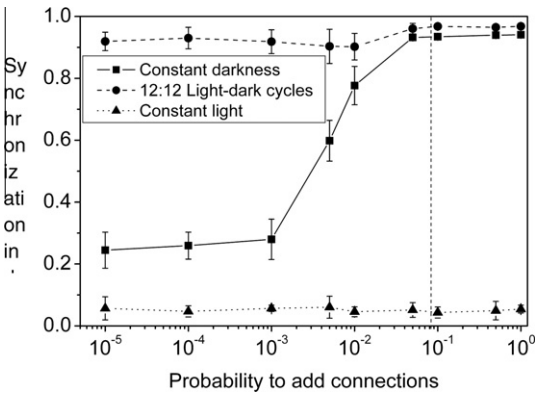

Fig. 6. The effect of different light schedules and SCN network topology on the synchronization index SI [125]. For each light schedule and p value, the mean (circle) and standard deviation (error bars) were computed from 10 network realizations.

4.3. Multicellular model of the core and shell regions

The SCN is organized into two structurally and functionally distinct subdivisions termed the core and the shell based on their neuropeptide content and network architecture [3,101]. Distinguishing feature of the core include neurons that co-produce VIP and GABA [82,83], a network characterized by short and long range connections between core neurons [94] as well as projections to shell neurons [56], and direct photic input [52]. By contrast, the shell has neurons that produce GABA but not VIP [82,83], a network characterized by short range connections between shell neurons without projections to core neurons [94], and no direct photic input [7]. Data concerning the spatial organization of self-sustained oscillators across the SCN network remain controversial [74,129].

Multicellular models that attempt to capture interactions between the core and shell regions have been developed [15,41,69]. We have developed a detailed multicellular model of structural and functional heterogeneities within the SCN [124]. The single cell model included a gene regulatory network submodel [67] that described the generation of autonomous oscillations and a firing rate-code submodel [123] that described electrical events on the SCN neuron membrane responsible for the generation of action potentials. The electrophysiology submodel accounted for the contributions of relevant ion channels as well as extracellular synaptic stimuli mediated by neurotransmitters that influenced membrane excitability and neural firing.

Intercellular couplings amongst SCN model neurons were mediated by VIP, GABA, and glutamate neurotransmitters. The VIP release rate was assumed to increase with the neural firing frequency, which was rhythmic and peaked during the circadian day. Intercellular and intracellular VIP signaling was formulated as in our previous single cell model (see Section 4.2). GABA was assumed to be rhythmically released as an increasing function of the firing frequency. GABA binding of its $GABA_A$ receptor was modeled as an increase in inhibitory post-synaptic currents through activation of Cl^- on the cell membrane and an increase in Cl^- influx into the cytosol. The amount of GABA observed by a particular neuron was averaged over the GABA released from the cells that had synaptic connections to that neuron. The glutamate pathway was modified from our previous study [123] to include circadian oscillations in glutamate uptake as well as the combined effects of AMPA and NMDA receptors. The model included the effects of photic stimuli conveyed via glutamate and PACAP neurotransmitters. Retinal input was modeled to directly affect core neurons, which in turn transmitted the signal to the shell population.

To mimic the spatial organization of the SCN, different connectivity schemes were used for the shell and core subdivisions (Fig. 7). A total of 425 neurons were distributed across the two regions such that the core contained 40% and the shell 60% of the neurons. The core was modeled as a small-world network with 169 heterogeneous cells placed on a 13×13 rectangular grid. Cell couplings within the core network were established by VIP and GABA signaling, with all cells producing GABA and only 50% of cells producing VIP. The shell was modeled with a nearest neighbor network to mimic the short range connectivity observed experimentally. An ensemble of 256 heterogeneous cells was placed on a 16×16 rectangular grid. Each neuron was assumed to establish connections with its four nearest neighbors via GABA intercellular signaling. Because the VPAC2 receptor is expressed by 90% of shell neurons [56], every neuron in the shell was assumed to be capable of receiving VIP signals from core neurons. We assigned a probability (p_{cs}) ranging from 0 to 1 according to which directed connections from VIP-synthesizing core neurons to shell neurons were introduced. The value $p_{cs} = 0$ produced two independent networks, whereas the value $p_{cs} = 1$ produced maximal connectivity between the two networks. Because GABA and VIP are co-expressed by VIP-synthesizing model neurons of the core, cell couplings extending from core to shell neurons were instigated by both neurotransmitters. As in our previous model (see Section 4.2), cellular heterogeneities were introduced through random perturbations in the basal *Per* transcription rate, the *Bmal1* transcription rate, and the *Bmal1* mRNA degradation rate. For each p_{cs} value, 10 network realizations were simulated to allow calculation of the necessary statistics.

The probability p_{cs} was varied to determine the effects of adding core-to-shell connections on system behavior under conditions of constant darkness. Synchronicity was

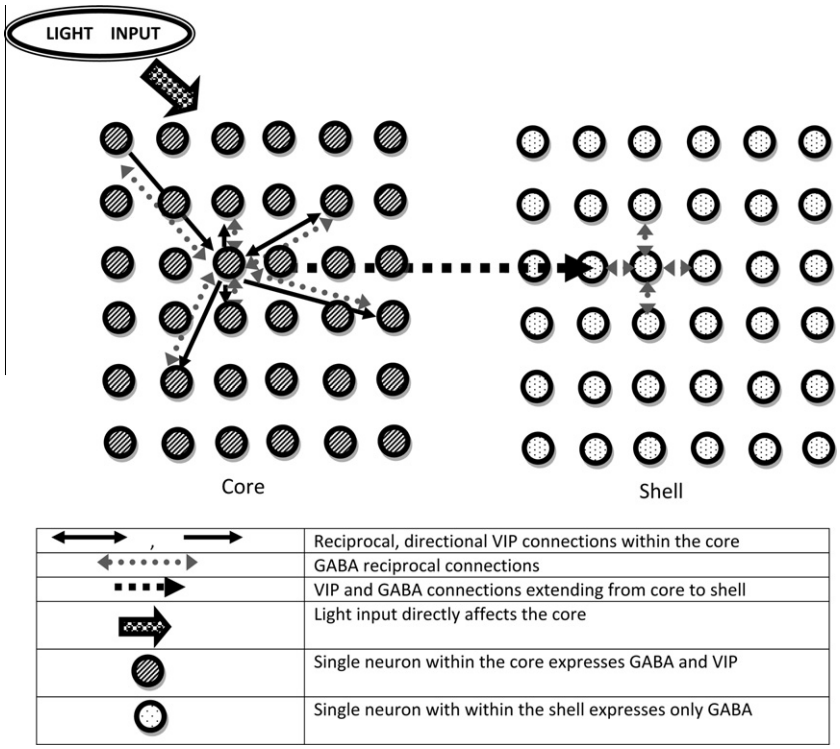

Fig. 7. Schematic representation of the heterogeneous cellular network used to mimic spatial organization of the SCN. The core was modeled as a small-world network with cell-to-cell couplings via VIP and GABA instigated signaling cascades. A locally connected architecture with nearest neighbor GABAergic couplings was used to describe the shell. The two SCN compartments were coupled via long range connections, randomly added according to a probability p_{cs}, which extended from core and to the shell. Only the core received direct light input.

evaluated at the end of 14 circadian cycles following the initiation of intercellular coupling. As expected, synchronicity remained constant across the core (SI = 0.9) over the entire range of probabilities (Fig. 8A). SI values for the shell monotonically increased as a function of p_{cs} and reached their upper asymptote of 0.9 for $p_{cs} = 0.05$ (Fig. 8A). Increasing cell-to-cell coordination across the shell affected the SI trend of the entire SCN network. While fluctuations in core period variability were regarded as insignificant, progressively larger p_{cs} values resulted in an increase in the average period and a decrease in period variability across the shell and the entire SCN until $p_{cs} = 0.05$ (Fig. 8B and C). Per mRNA and firing rate profiles of 20 neurons randomly selected from the SCN population showed that core-to-shell connectivity generated at $p_{cs} = 0.05$ was sufficient to produce highly phased synchronized oscillations across the network (Fig. 8D and E). The average period across the synchronized SCN population at the end of 14 cycles was 23.5 h and the standard deviation was 0.3 h, while the average period across uncoupled self-sustained oscillators was 22.5 h and the distribution of periods among these oscillators had a standard deviation of 0.7 h (Fig. 8F). These model predictions are consistent with experiments demonstrating reduced periods and increased period variability across the SCN population in the absence of functional intercellular couplings [20,129].

The probability p_{cs} was varied for different light schedules to determine their combined effects on system

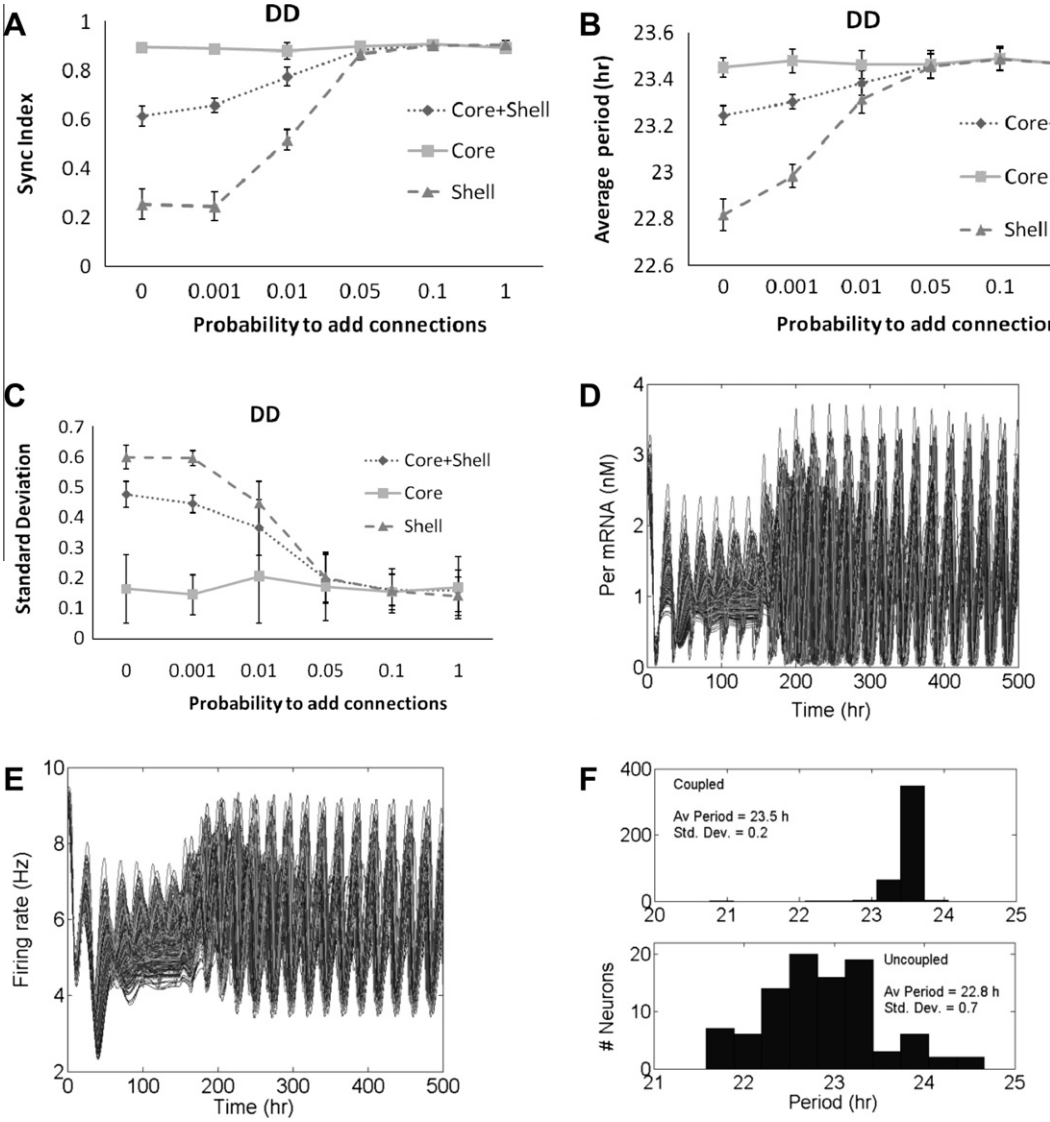

Fig. 8. The effect of core-to-shell connectivity under conditions of constant darkness. For each p_{cs}, value the mean (circle) and standard deviation (error bars) were computed across 10 independent runs. The SI value (A), the average period of the population (B), and the period variability (C) as a function of the probability p_{cs} were calculated across the core, shell and entire SCN networks at the end of 14 simulations cycles. *Per* mRNA (D) and firing rate (E) profiles of 20 randomly selected neurons for $p_{cs} = 0.05$ when cell-to-cell coupling was introduced at 150 h. (F) Period distribution at the 14th cycle obtained with $p_{cs} = 0.05$ for all cells within the coupled population (top panel) and for self-sustained oscillators in the uncoupled population (lower panel).

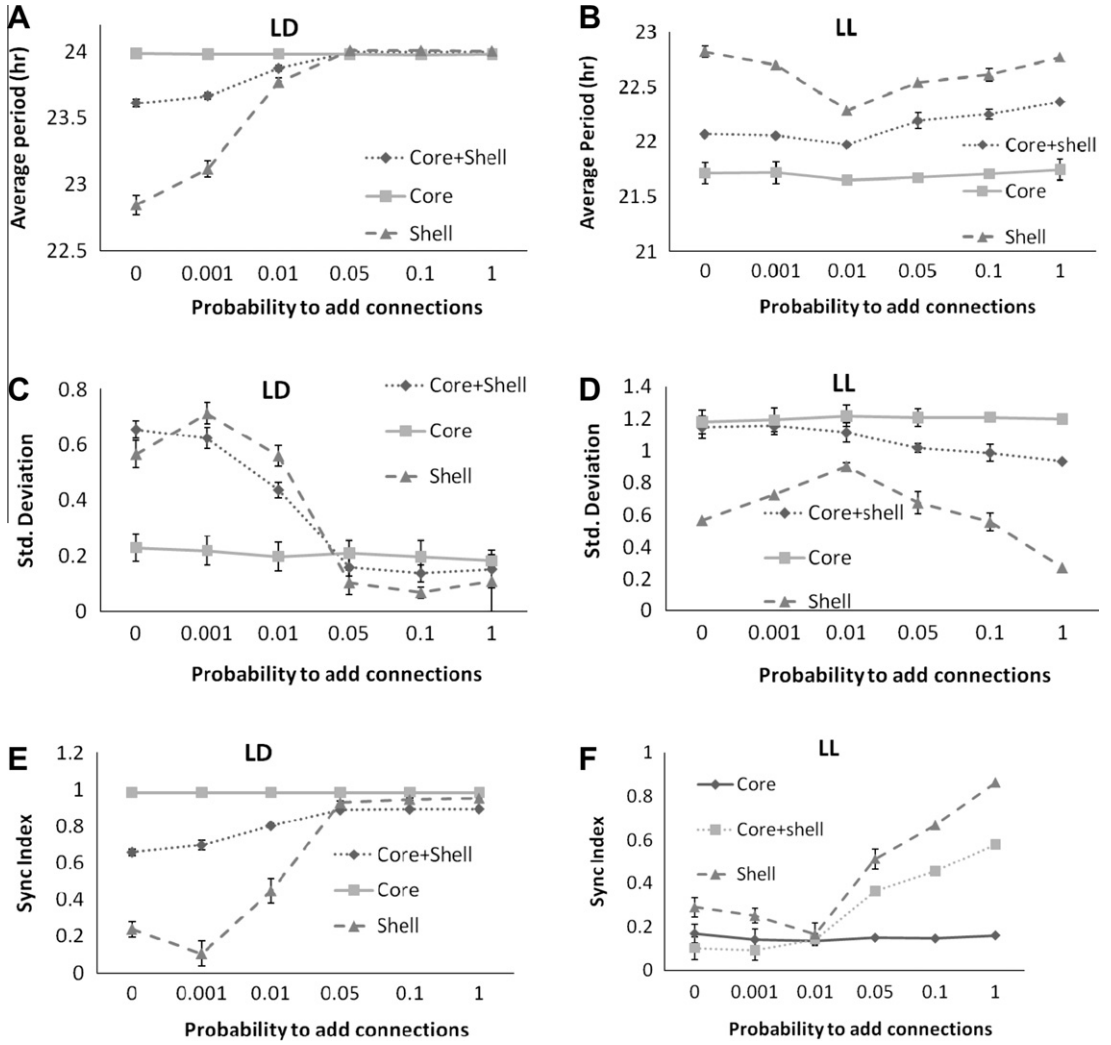

Fig. 9. The combined effects of different photic stimuli and core-to-shell connectivity. For each p_{cs} value, the mean (circle) and standard deviation (error bars) were computed across 10 independent runs. The average period (A), period variability (C) and SI value (E) as a function of the probability p_{cs} across the core, shell and entire SCN networks in LD cycles. The average period (B), period variability (D) and SI value (F) as a function of the probability p_{cs} across the core, shell and entire SCN networks in LL.

behavior. As p_{cs} was increased in LD cycles, the average period increased and period variability decreased across the shell and the entire SCN network with asymptotic values reached at $p_{cs} = 0.05$ (Fig. 9A and C). By contrast, the LL schedule did not produce distinct period trends across the shell population for the range of probabilities tested (Fig. 9B and D). Synchronization across the core network remained approximately constant for each light schedule, with SI = 0.96 for LD (Fig. 9E) and SI = 0.15 for LL (Fig. 9F). In LD cycles, SI values of the shell network monotonically increased with increasing p_{cs}, with a maximal SI value of 0.94 achieved at $p_{cs} = 0.05$. Compared to LD and DD (Fig. 8A), exposure to LL produced decreased SI values across the entire SCN population for the range of probabilities tested. The modest increase in synchronicity with increasing p_{cs} can be attributed to improved coordination of the shell population upon introduction of core-to-shell links. The small SI values predicted for both the core and shell networks are consistent with experiments reporting disrupted circadian rhythms in the two regions due to constant light exposure [13].

5. Conclusion and future directions

The circadian clock generates 24 h rhythms that drive a broad range of physiological and behavioral processes in diverse organisms. In mammal, the core clock located in the suprachiasmatic nucleus (SCN) of the hypothalamus consists of approximately 20,000 heterogeneous neurons that coordinate their behavior to generate a coherent overall rhythm. While the molecular mechanisms involved in circadian rhythm generation at the single cell level are well characterized, the intercellular mechanisms that allow large populations of coupled neurons to synchronize their activities remain poorly understood. The goal of this paper

was to provide a review of mathematical modeling efforts aimed at developing multicellular descriptions of the circadian core clock. With a focus on the mammalian clock due to its relevance in human performance and health, we argued that detailed biophysical models comprised of detailed single cell descriptions, plausible descriptions of intracellular and intercellular neurotransmitter signaling pathways, and heterogeneous descriptions of single cell behavior and cell-to-cell connectivity are preferred for integrating experimental data and understanding system design principles. A review of our own modeling work showed that limited long range connections combined with more dense local coupling was sufficient to coordinate heterogeneous cell populations organized in functionally distinct SCN regions.

While multicellular modeling of circadian neuron populations has seen rapid advancement, considerable work remains to develop comprehensive models for data integration, analysis, and prediction. Several modeling problems that warrant additional work by the circadian research community are described below. Collaborations between experimentalists and modelers will be essential for development and validation of these models.

- Construction of increasingly detailed single cell models that capture relevant gene regulatory and electrophysiological behavior for connecting molecular components to system behavior. Recently developed gene regulatory [80], electrophysiology [107], and combined gene regulatory-electrophysiology [123] models are notable steps in this direction.
- Development of intracellular and intercellular signaling models that mechanistically describe the action of relevant neurotransmitters and light on single cell and population behavior. Proposed models of VIP [45,116] and combined VIP/GABA/glutamate [123,126] signaling demonstrate the potential of this approach compared to empirical coupling schemes.
- Construction of neural network topologies that better capture non-uniform cell-to-cell communication than current models, which are restricted to standard topologies and static coupling. Progress towards this goal will be facilitated by the analysis and simulation of experimentally derived spatial organization [29] and coupling patterns, including those that evolve with season [76,86] and during circadian system development [25] and ageing [30].
- Development of cell population simulations that capture single cell heterogeneity on a more mechanistic basis than current models, which phenomenologically ascribe heterogeneity in cellular phenotype to random variations in chosen model parameters. Such simulations could be advanced by experimental determination of the molecular sources of cellular variability [114] as well as the development of stochastic simulation techniques [28,121] that allow the phenotype of a particular neuron to vary with time.
- Development of improved simulation methods for complex multicellular models, including those that describe three dimensional tissues, contain large ensembles of detailed cell models, include stochastic variability in single cell properties, and allow time-varying network topologies. Deterministic [16] and stochastic [57] simulation techniques developed for other multicellular systems could be leveraged for this purpose.

Acknowledgements

The authors would like to acknowledge the contributions of the following collaborators to the results in Section 4: Francis J. Doyle III (University of California, Santa Barbara), Erik D. Herzog (Washington University), Tze-Leung To (University of California, San Francisco), and Christina Vasalou (Novartis). This work was supported by the National Institutes of Health (Grants GM078993 and 1R01GM096873-01).

References

[1] Abe M, Herzog ED, Yamazaki S, Straume M, Tei H, Sakaki Y, et al. Circadian rhythms in isolated brain regions. J Neurosci 2002; 22:350–6.
[2] Abraham U, Granada AE, Westermark PO, Heine M, Kramer A, Herzel H. Coupling governs entrainment range of circadian clocks. Mol Syst Biol 2010;6:438.
[3] Abrahamson EE, Moore RY. Suprachiasmatic nucleus in the mouse: retinal innervation, intrinsic organization and efferent projections. Brain Res 2001;916:172–91.
[4] Achermann P, Kunz H. Modeling circadian rhythm generation in the suprachiasmatic nucleus with locally coupled self-sustained oscillators: phase shifts and phase response curves. J Biol Rhythms 1999;14:460–8.
[5] Albert R, Barabási A-L. Statistical mechanics of complex networks. Rev Mod Phys 2002;74:47–97.
[6] Antle MC, Foley DK, Foley NC, Silver R. Gates and oscillators: a network model of the brain clock. J Biol Rhythms 2003;18:339–50.
[7] Antle MC, Silver R. Orchestrating time: arrangements of the brain circadian clock. Trends Neurosci 2005;28:145–51.
[8] Aton SJ, Block GD, Tei H, Yamazaki S, Herzog ED. Plasticity of circadian behavior and the suprachiasmatic nucleus following exposure to non-24-hour light cycles. J Biol Rhythms 2004;19(3): 198–207.
[9] Aton SJ, Colwell CS, Harmar AJ, Waschek J, Herzog ED. Vasoactive intestinal polypeptide mediates circadian rhythmicity and synchrony in mammalian clock neurons. Nat Neurosci 2005;8: 476–83.
[10] Aton SJ, Herzog ED. Come together, right. . .now: synchronization of rhythms in a mammalian circadian clock. Neuron 2005;48:531–4.
[11] Aton SJ, Huettner JE, Straume M, Herzog ED. GABA and Gi/o differentially control circadian rhythms and synchrony in clock neurons. Proc Natl Acad Sci 2006;103:19188–93.
[12] Barabási A-L, Albert R. Emergence of scaling in random networks. Science 1999;286:509–12.
[13] Beaulé C, Houle L, Amir S. Expression profiles of PER2 immunoreactivity within the shell and core regions of the rat suprachiasmatic nucleus. J Mol Neurosci 2003;21:133–47.
[14] Belenky MA, Yarom Y, Pickard GE. Heterogeneous expression of gamma-aminobutyric acid and gamma-aminobutyric acid-associated receptors and transporters in the rat suprachiasmatic nucleus. J Comput Neurol 2008;506:708–32.
[15] Bernard S, Gonze D, Čajavec B, Herzel H, Kramer A. Synchronization-induced rhythmicity of circadian oscillators in the suprachiasmatic nucleus. PLoS Comput Biol 2007;3:e68.
[16] Bold KA, Zou Y, Kevrekidis I, Henson M. Efficient simulation of coupled biological oscillators through equation-free uncertainty quantification. J Math Biol 2007;55:331–52.
[17] Brown SA, Fleury-Olela F, Nagoshi E, Hauser C, Juge C, Meier CA, et al. The period length of fibroblast circadian gene expression varies widely among human individuals. PLoS Biol 2005;3:e338.
[18] Brown TM, Hughes AT, Piggins HD. Gastrin-releasing peptide promotes suprachiasmatic nuclei cellular rhythmicity in the absence of vasoactive intestinal polypeptide-VPAC2 receptor signaling. J Neurosci 2005;25:11155–64.

[19] Brown TM, Piggins HD. Electrophysiology of the suprachiasmatic circadian clock. Prog Neurobiol 2007;82:229–55.
[20] Brown TM, Piggins HD. Spatiotemporal heterogeneity in the electrical activity of suprachiasmatic nuclei neurons and their response to photoperiod. J Biol Rhythms 2009;24:44–54.
[21] Bush WS, Siegelman HT. Circadian synchrony in networks of protein rhythm driven neurons. Complexity 2006;12:67–72.
[22] Card JP, Moore RY. The suprachiasmatic nucleus of the golden hamster: immunohistochemical analysis of cell and fiber distribution. Neuroscience 1984;13:415–31.
[23] Castel M, Morris JF. Morphological heterogeneity of the GABAergic network in the suprachiasmatic nucleus, the brain's circadian pacemaker. J Anat 2000;196:1–13.
[24] Choi HJ, Lee CJ, Schroeder A, Kim YS, Jung SH, Kim JS, et al. Excitatory actions of GABA in the suprachiasmatic nucleus. J Neurosci 2008;28:5450–9.
[25] Ciarleglio CM, Axley JC, Strauss BR, Gamble KL, McMahon DG. Perinatal photoperiod imprints the circadian clock. Nat Neurosci 2011;14:25–7.
[26] Daikoku S, Hisano S, Kagotani Y. Neuronal associations in the rat suprachiasmatic nucleus demonstrated by immunoelectron microscopy. J Comput Neurol 1992;325:559–71.
[27] Diambra L, Malta CP. Modeling the emergence of circadian rhythms in a clock neuron network. PLoS ONE 2012;7:e33912.
[28] Edwards B, Waterhouse J, Reilly T. The effects of circadian rhythmicity and time-awake on a simple motor task. Chronobiol Int 2007;24:1109–24.
[29] Evans JA, Leise TL, Castanon-Cervantes O, Davidson AJ. Intrinsic regulation of spatiotemporal organization within the suprachiasmatic nucleus. PLoS ONE 2011;6:e15869.
[30] Farajnia S, Michel S, Deboer T, vanderLeest HT, Houben T, Rohling JH, et al. Evidence for neuronal desynchrony in the aged suprachiasmatic nucleus clock. J Neurosci 2012;32:5891–9.
[31] Forger DB, Peskin CS. A detailed predictive model of the mammalian circadian clock. Proc Natl Acad Sci 2003;100: 14806–11.
[32] François P. A model for the neurospora circadian clock. Biophys J 2005;88:2369–83.
[33] Fukuda H, Tokuda I, Hashimoto S, Hayasaka N. Quantitative analysis of phase wave of gene expression in the mammalian central circadian clock network. PLoS ONE 2010;6:e23568.
[34] Garcia-Ojalvo J, Elowitz MB, Strogatz SH. Modeling a synthetic multicellular clock: repressilators coupled by quorum sensing. Proc Natl Acad Sci 2004;101:10955–60.
[35] Gillette M, Mitchell J. Signaling in the suprachiasmatic nucleus: selectively responsive and integrative. Cell Tissue Res 2002;309: 99–107.
[36] Ginty DD, Glowacka D, Bader DS, Hidaka H, Wagner JA. Induction of immediate early genes by Ca2+ influx requires cAMP-dependent protein kinase in PC12 cells. J Biol Chem 1991;266:17454–8.
[37] Goldbeter A. A model for circadian oscillations in the drosophila period protein (PER). Proc R Soc Lond B Biol Sci 1995;261: 319–24.
[38] Goldbeter A. Biochemical oscillations and cellular rhythms: the molecular bases of periodic and chaotic behavior. 2nd ed. Cambridge: University Press; 1996.
[39] Gonze D, Bernard S, Waltermann C, Kramer A, Herzel H. Spontaneous synchronization of coupled circadian oscillators. Biophys J 2005;89:120–9.
[40] Gonze D, Leloup J-C, Goldbeter A. Theoretical models for circadian rhythms in Neurospora and Drosophila. CR Acad Sci – Ser – Sci Vie 2000;323:57–67.
[41] Hafner M, Koeppl H, Gonze D. Effect of network architecture on synchronization and entrainment properties of the circadian oscillations in the suprachiasmatic nucleus. PLoS Comput Biol 2010;8:e1002419.
[42] Hamada T, LeSauter J, Venuti JM, Silver R. Expression of period genes: rhythmic and nonrhythmic compartments of the suprachiasmatic nucleus pacemaker. J Neurosci 2001;21:7742–50.
[43] Hannibal J, Ding JM, Chen D, Fahrenkrug J, Larsen PJ, Gillette MU, et al. Pituitary adenylate cyclase-activating peptide (PACAP) in the retinohypothalamic tract: a potential daytime regulator of the biological clock. J Neurosci 1997;17:2637–44.
[44] Hannibal J, Moller M, Ottersen OP, Fahrenkrug J. PACAP and glutamate are co-stored in the retinohypothalamic tract. J Comput Neurol 2000;418:147–55.
[45] Hao H, Zak DE, Sauter T, Schwaber J, Ogunnaike BA. Modeling the VPAC2 activated cAMP/PKA pathway: from receptor to circadian clock induction. Biophys J 2006;90:1560–71.
[46] Hardin PE. Molecular genetic analysis of circadian timekeeping in *Drosophila*. Adv Genet 2011;74:141–73.
[47] Harmar AJ, Marston HM, Shen S, Spratt C, West KM, Sheward WJ, et al. The VPAC2 receptor is essential for circadian function in the mouse suprachiasmatic nuclei. Cell 2002;109:497–508.
[48] Hendricks JC, Lu S, Kume K, Yin JC, Yang Z, Sehgal A. Gender dimorphism in the role of cycle (BMAL1) in rest, rest regulation, and longevity in *Drosophila melanogaster*. J Biol Rhythms 2003;18:12–25.
[49] Henson MA. Modeling the synchronization of yeast respiratory oscillations. J Theor Biol 2004;231:443–58.
[50] Herzog ED, Aton SJ, Numano R, Sakaki Y, Tei H. Temporal precision in the mammalian circadian system: a reliable clock from less reliable neurons. J Biol Rhythms 2004;19:35–46.
[51] Herzog ED, Takahashi JS, Block GD. Clock controls circadian period in isolated suprachiasmatic nucleus neurons. Nat Neurosci 1998;1:708–13.
[52] Ibata Y, Takahashi Y, Okamura H, Kawakami F, Terubayashi H, Kubo T, et al. Vasoactive intestinal Peptide (VIP)-like immunoreactive neurons located in the eat suprachiasmatic nucleus receive a direct retinal projection. Neurosci Lett 1989;97:1–5.
[53] Ikeda M, Sugiyama T, Wallace CS, Gompf HS, Yoshioka T, Miyawaki A, et al. Circadian dynamics of cytosolic and nuclear Ca2+ in single suprachiasmatic nucleus neurons. Neuron 2003;38:253–63.
[54] Itri J, Colwell CS. Regulation of inhibitory synaptic transmission by vasoactive intestinal peptide (VIP) in the mouse suprachiasmatic nucleus. J Neurophysiol 2003;90:1589–97.
[55] Itri JN, Michel S, Vansteensel MJ, Meijer JH, Colwell CS. Fast delayed rectifier potassium current is required for circadian neural activity. Nat Neurosci 2005;8:650–6.
[56] Kalamatianos T, Kalló I, Piggins HD, Coen CW. Expression of VIP and/or PACAP Receptor mRNA in peptide synthesizing cells within the suprachiasmatic nucleus of the rat and in its efferent target sites. J Comp Neurol 2004;475:19–35.
[57] Kavousanakis ME, Liu P, Boudouvis AG, Lowengrub J, Kevrekidis IG. Efficient coarse simulation of a growing avascular tumor. Phys Rev E 2012;85:031912–22.
[58] King VM, Chahad-Ehlers S, Shen S, Harmar AJ, Maywood ES, Hastings MH. A hVIPR transgene as a novel tool for the analysis of circadian function in the mouse suprachiasmatic nucleus. Eur J Neurosci 2003;17:822–32.
[59] Klein DC, Moore RY, Reppert SM. Suprachiasmatic nucleus: the mind's clock. New York: Oxford University Press; 1991.
[60] Kondratova AA, Kondratov RV. The circadian clock and pathology of the ageing brain. Nat Rev Neurosci 2012;13:325–35.
[61] Kuhlman SJ, McMahon DG. Rhythmic regulation of membrane potential and potassium current persists in SCN neurons in the absence of environmental input. Eur J Neurosci 2004;20: 1113–7.
[62] Kunz H, Achermann P. Simulation of circadian rhythm generation in the suprachiasmatic nucleus with locally coupled self-sustained oscillators. J Theor Biol 2003;224(1):63–78.
[63] Kuramoto Y. Chemical oscillations, waves, and turbulence. Berlin: Springer; 1984.
[64] Leak RK, Moore RY. Topographic organization of suprachiasmatic nucleus projection neurons. J Comput Neurol 2007;433: 312–34.
[65] Lee K, Loros JJ, Dunlap JC. Interconnected feedback loops in the neurospora circadian system. Science 2000;289:107–10.
[66] Leloup J-C, Goldbeter A. A Model for circadian rhythms in *Drosophila* incorporating the formation of a complex between the PER and TIM proteins. J Biol Rhythms 1998;13:70–87.
[67] Leloup J-C, Goldbeter A. Toward a detailed computational model for the mammalian circadian clock. Proc Natl Acad Sci 2003;100: 7051–6.
[68] Leloup J-C, Gonze D, Goldbeter A. Limit cycle models for circadian rhythms based on transcriptional regulation in *Drosophila* and *Neurospora*. J Biol Rhythms 1999;14:433–48.
[69] Li Y, Liu Z, Zhang J, Wang R, Chen L. Synchronisation mechanisms of circadian rhythms in the suprachiasmatic nucleus. IET Syst Biol 2009;3:100–12.
[70] Liu C, Reppert SM. GABA synchronizes clock cells within the suprachiasmatic circadian clock. Neuron 2000;25:123–8.
[71] Liu C, Weaver DR, Strogatz SH, Reppert SM. Cellular construction of a circadian clock: period determination in the suprachiasmatic nuclei. Cell 1997;91:855–60.
[72] Low-Zeddies SS, Takahashi JS. Chimera analysis of the clock mutation in mice shows that complex cellular integration determines circadian behavior. Cell 2001;105:25–42.

[73] Lundkvist GB, Kwak Y, Davis EK, Tei H, Block GD. A calcium flux is required for circadian rhythm generation in mammalian pacemaker neurons. J Neurosci 2005;25:7682–6.
[74] Maywood ES, Reddy AB, Wong GK, O'Neill JS, O'Brien JA, McMahon DG, et al. Synchronization and maintenance of timekeeping in suprachiasmatic circadian clock cells by neuropeptidergic signaling. Curr Biol 2006;16:599–605.
[75] McClung CA. Circadian genes, rhythms and the biology of mood disorders. Pharmacol Ther 2007;114:222–32.
[76] Meijer JH, Michel S, Vanderleest HT, Rohling JH. Daily and seasonal adaptation of the circadian clock requires plasticity of the SCN neuronal network. Eur J Neurosci 2010;32:2143–51.
[77] Meredith AL, Wiler SW, Miller BH, Takahashi JS, Fodor AA, et al. BK calcium-activated potassium channels regulate circadian behavioral rhythms and pacemaker output. Natur Neurosci 2006; 9:1041–9.
[78] Merrow M, Roenneberg T, Macino G, Franchi L. A fungus among us: the *Neurospora crassa* circadian system. Semin Cell Dev Biol 2001;12:279–85.
[79] Mirollo RE, Strogatz SH. Synchronization of pulse-coupled biological oscillators. SIAM J Appl Math 1990;50:1645–62.
[80] Mirsky HP, Liu AC, Welsh DK, Kay SA, Doyle FJ. A model of the cell-autonomous mammalian circadian clock. Proc Natl Acad Sci 2009;106:11107–12.
[81] Moga MM, Moore RY. Organization of neural inputs to the suprachiasmatic nucleus in the rat. J Comput Neurol 1997; 389:508–34.
[82] Moore KA, Kohno T, Karchewski LA, Scholz J, Baba H, Woolf CJ. Partial peripheral nerve injury promotes a selective loss of GABAergic inhibition in the superficial dorsal horn of the spinal cord. J Neurosci 2002;22:6724–31.
[83] Moore RY, Speh JC, Leak RK. Suprachiasmatic nucleus organization. Cell Tissue Res 2004;309:89–98.
[84] Morin LP. SCN organization reconsidered. J Biol Rhythms 2007;22:3–13.
[85] Nagai T, Terada TP, Sasai M. Synchronization of circadian oscillation of phosphorylation level of KaiC *In Vitro*. Biophys J 2010; 98:2469–77.
[86] Naito E, Watanabe T, Tei H, Yoshimura T, Ebihara S. Reorganization of the suprachiasmatic nucleus coding for day length. J Biol Rhythms 2008;23:140–9.
[87] Netoff TI, Clewley R, Arno S, Keck T, White JA. Epilepsy in small-world networks. J Neurosci 2004;24:8075–83.
[88] Newman MEJ. Models of the small world. J Stat Phys 2000; 101:819–41.
[89] Novak CM, Ehlen JC, Paul KN, Fukuhara C, Albers HE. Light and GABAA receptor activation alter period mRNA levels in the SCN of diurnal nile grass rats. Eur J Neurosci 2006;24:2843–52.
[90] Oda GA, Friesen WO. A model for 'splitting' of running-wheel activity in hamsters. J Biol Rhythms 2002;17:76–88.
[91] Oda GA, Friesen WO. Modeling two-oscillator circadian systems entrained by two environmental cycles. PLoS ONE 2011;6:e23895.
[92] Ohta H, Yamazaki S, McMahon DG. Constant light desynchronizes mammalian clock neurons. Nat Neurosci 2006;8:267–9.
[93] Paul KN, Fukuhara C, Karom M, Tosini G, Albers HE. AMPA/Kainate receptor antagonist DNQX blocks the acute increase of Per2 mRNA levels in most but not all areas of the SCN. Mol Brain Res 2005;139:129–36.
[94] Pennartz CM, De Jeu MT, Geurtsen AM, Sluiter AA, Hermes ML. Electrophysiological and morphological heterogeneity of neurons in slices of rat suprachiasmatic nucleus. J Physiol 1998;506:775–93.
[95] Pennartz CMA, de Jeu MTG, Bos NP, Schaap J, Geurtsen AM. Diurnal modulation of pacemaker potentials and calcium current in the mammalian circadian clock. Nature 2002;416:286–90.
[96] Petri B, Stengl M. Phase response curves of a molecular model oscillator: implications for mutual coupling of paired oscillators. J Biol Rhythms 2001;16:125–41.
[97] Pokhilko A, Fernández AP, Edwards KD, Southern MM, Halliday KJ, Millar AJ. The clock gene circuit in *Arabidopsis* includes a repressilator with additional feedback loops. Mol Syst Biol 2012; 8:574.
[98] Quintero JE, Kuhlman SJ, McMahon DG. The biological clock nucleus: a multiphasic oscillator network regulated by light. J Neurosci 2003;23:8070–6.
[99] Reppert SM, Weaver DR. Molecular analysis of mammalian circadian rhythms. Annu Rev Physiol 2001;63:647–76.
[100] Reppert SM, Weaver DR. Coordination of circadian timing in mammals. Nature 2002;418:935–41.
[101] Robert MY. Entrainment pathways and the functional organization of the circadian system. Amsterdam: Elsevier; 1996.
[102] Roybal K, Theobold D, Graham A, DiNieri JA, Russo SJ, Krishnan V, et al. Mania-like behavior induced by disruption of CLOCK. Proc Natl Acad Sci 2007;104:6406–11.
[103] Ruoff P, Vinsjevik M, Monnerjahn C, Rensing L. The Goodwin model: simulating the effect of light pulses on the circadian sporulation rhythm of *Neurospora crassa*. J Theor Biol 2001;209:29–42.
[104] Rust MJ, Markson JS, Lane WS, Fisher DS, O'Shea EK. Ordered phosphorylation governs oscillation of a three-protein circadian clock. Science 2007;318:809–12.
[105] Salomé PA, McClung CR. The *Arabidopsis thaliana* clock. J Biol Rhythms 2004;19:425–35.
[106] Shinohara K, Honma S, Katsuno Y, Abe H, Honma K. 2 Distinct oscillators in the rat suprachiasmatic nucleus *In-vitro*. Proc Natl Acad Sci 1995;92:7396–400.
[107] Sim CK, Forger DB. Modeling the electrophysiology of suprachiasmatic nucleus neurons. J Biol Rhythms 2007;22:445–53.
[108] Smolen P, Baxter DA, Byrne JH. Modeling circadian oscillations with interlocking positive and negative feedback loops. J Neurosci 2001;21:6644–56.
[109] Sporns O, Chialvo DR, Kaiser M, Hilgetag CC. Organization, development and function of complex brain networks. Trends Cognit Sci 2004;8:418–25.
[110] Stelling J, Sauer U, Szallasi Z, Doyle FJ. Robustness of cellular functions. Cell 2004;118:675–85.
[111] Strecker GJ, Wuarin J-P, Dudek FE. GABAA-mediated local synaptic pathways connect neurons in the rat suprachiasmatic nucleus. J Neurophysiol 1997;78:2217–20.
[112] Strogatz SH. From Kuramoto to Crawford: exploring the onset of synchronization in populations of coupled oscillators. Physica D 2000;143:1–20.
[113] Strogatz SH. Exploring complex networks. Nature 2001; 410:268–76.
[114] Suter DM, Molina N, Gatfield D, Schneider K, Schibler U, Naef F. Mammalian genes are transcribed with widely different bursting kinetics. Science 2011;332:472–4.
[115] Tischkau SA, Mitchell JW, Tyan SH, Buchanan GF, Gillette MU. Ca2+/cAMP response element-binding protein (CREB)-dependent activation of Per1 is required for light-induced signaling in the suprachiasmatic nucleus circadian clock. J Biol Chem 2003; 278:718–23.
[116] To T-L, Henson MA, Herzog ED, Doyle FJ. A molecular model for intercellular synchronization in the mammalian circadian clock. Biophys J 2007;92:3792–803.
[117] Tousson E, Meissl H. Suprachiasmatic nuclei grafts restore the circadian rhythm in the paraventricular nucleus of the hypothalamus. J Neurosci 2004;24:2983–8.
[118] Tyson JJ, Hong CI, Dennis Thron C, Novak B. A simple model of circadian rhythms based on dimerization and proteolysis of PER and TIM. Biophys J 1999;77:2411–7.
[119] Ueda HR, Hagiwara M, Kitano H. Robust oscillations within the interlocked feedback model of drosophila circadian rhythm. J Theor Biol 2001;210:401–6.
[120] Ueda HR, Matsumoto A, Kawamura M, Iino M, Tanimura T, Hashimoto S. Genome-wide transcriptional orchestration of circadian rhythms in *Drosophila*. J Biol Chem 2002;277:14048–52.
[121] Ullner E, Buceta J, Diez-Noguera A, Garcia-Ojalvo J. Noise-induced coherence in multicellular circadian clocks. Biophys J 2009;96:3573–81.
[122] Vandenpol AN, Tsujimoto KL. Neurotransmitters of the hypothalamic suprachiasmatic nucleus – immunocytochemical analysis of 25 neuronal antigens. Neuroscience 1985;15:1049–86.
[123] Vasalou C, Henson MA. A multiscale model to investigate circadian rhythmicity of pacemaker neurons in the suprachiasmatic nucleus. PLoS Comput Biol 2010;6:e1000706.
[124] Vasalou C, Henson MA. A multicellular model for differential regulation of circadian signals in the shell and core regions of the SCN. J Theor Biol 2011;288:44–56.
[125] Vasalou C, Herzog ED, Henson MA. Small-world network models of intercellular coupling predict enhanced synchronization in the suprachiasmatic nucleus. J Biol Rhythms 2009;24:243–54.
[126] Vasalou C, Herzog ED, Henson MA. Multicellular model for intercellular synchronization in circadian neural networks. Biophys J 2011;101:12–20.
[127] von Gall C, Duffield GE, Hastings MH, Kopp MD, Dehghani F, Korf HW, et al. CREB in the mouse SCN: a molecular interface coding the

phase-adjusting stimuli light, glutamate, PACAP, and melatonin for clockwork access. J Neurosci 1998;18:10389–97.
[128] Watts DJ, Strogatz SH. Collective dynamics of small-world networks. Nature 1998;393:440–2.
[129] Webb AB, Angelo N, Huettner JE, Herzog ED. Intrinsic, nondeterministic circadian rhythm generation in identified mammalian neurons. Proc Natl Acad Sci 2009;106:16493–8.
[130] Welsh DK, Logothetis DE, Meister M, Reppert SM. Individual neurons dissociated from rat suprachiasmatic nucleus express independently phased circadian firing rhythms. Neuron 1995;14:697–706.
[131] Winfree AT. Biological rhythms and the behavior of populations of coupled oscillators. J Theor Biol 1967;16:15–42.
[132] Winfree AT. The geometry of biological time. 2nd ed. New York: Springer-Verlag; 2001.
[133] Xu Y, Padiath QS, Shapiro RE, Jones CR, Wu SC, Saigoh N, et al. Functional consequences of a CKI[delta] mutation causing familial advanced sleep phase syndrome. Nature 2005;434:640–4.